ACS APPLIED MATERIALS & INTERFACES

Research Article

www.acsami.org

Three-Dimensional Nanoporous Graphene-Carbon Nanotube Hybrid Frameworks for Confinement of SnS_2 Nanosheets: Flexible and Binder-Free Papers with Highly Reversible Lithium Storage

Longsheng Zhang,[†] Yunpeng Huang,[†] Youfang Zhang,[†] Wei Fan,[*,‡] and Tianxi Liu[*,†,‡]

[†]State Key Laboratory of Molecular Engineering of Polymers, Department of Macromolecular Science, Fudan University, Shanghai 200433, People's Republic of China

[‡]State Key Laboratory of Modification of Chemical Fibers and Polymer Materials, College of Materials Science and Engineering, Donghua University, Shanghai 201620, People's Republic of China

Supporting Information

ABSTRACT: The practical applications of transition-metal dichalcogenides for lithium-ion batteries are severely inhibited by their inferior structural stability and electrical conductivity, which can be solved by optimizing these materials to nanostructures and confining them within conductive frameworks. Thus, we report a facile approach to prepare flexible papers with SnS_2 nanosheets (SnS_2 NSs) homogeneously dispersed and confined within the conductive graphene-carbon nanotube (CNT) hybrid frameworks. The confinement of SnS_2 NSs in graphene-CNT matrixes not only can effectively prevent their aggregation during the discharge−charge procedure, but also can assist facilitating ion transfer across the interfaces. As a result, the optimized SGC papers give an improved capacity of 1118.2 mA h g^{-1} at 0.1 A g^{-1} along with outstanding stability. This report demonstrates the significance of employing graphene-CNT matrixes for confinement of various active materials to fabricate flexible electrode materials.

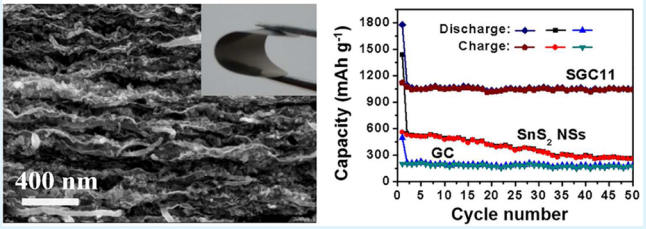

KEYWORDS: *SnS_2 nanosheets, graphene, carbon nanotubes, confinement, flexible anodes, lithium-ion batteries*

1. INTRODUCTION

Nowadays, lithium-ion batteries (LIBs) have been intensively pursued to alleviate the ever-growing demand for efficient energy storage.[1] To fulfill the demands, it has put forward the development of LIBs with higher specific capacity and better cycling life.[2] Currently, as the most commonly used anode materials for LIBs, the commercialized graphite cannot accommodate the requirement for next-generation LIBs owing to their inferior theoretical capacity.[3] Thus, the research for alternative anode materials with higher capacity has received more and more attention.[4−8] Recently, a variety of two-dimensional (2D) metal dichalcogenides (e.g., WS_2, SnS_2, and so on) with higher theoretical capacities are studied as potential anodes of the high-power LIBs.[9−14] Notably, SnS_2 has a sandwiched structure composed of one tier of Sn atom and double tiers of S atoms.[15−17] Additionally, the interlayer spacing between SnS_2 layers is suitable for fast insertion/extraction of lithium ions.[18] Nevertheless, the applications of SnS_2 are held back by their interior structural stability and electrical conductivity.[19−22] Besides, it is very hard to reach complete intercalation of restacked SnS_2 nanosheets, thus resulting in reduced electrochemical performance.[23]

To address these issues, optimizing the SnS_2 materials to nanostructures and constructing hybrid structures with SnS_2 confined in conductive carbonaceous matrix are effective approaches to accommodate the volumetric expansion and enhance the cyclic stability of SnS_2 nanomaterials.[24−26] Compared to other carbon nanomaterials, graphene is considered as an ideal matrix to disperse and confine active materials due to its 2D layered structures, large surface areas, and superior electrical conductivity.[27−29] Nevertheless, restacking of graphene sheets hampers the utilization of the great potential of graphene.[30,31] Thus, one effective strategy is to incorporate carbon nanotubes (CNTs) between graphene sheets, which will prevent the restacking of graphene.[32] With addition of CNTs, the three-dimensional (3D) graphene-CNT composites exhibit greatly enhanced conductivity and surface areas compared with neat graphene.[33,34] Nevertheless, the majority of reports about graphene-CNT composites involves addition of cosurfactant that decreases their conductivity[35] or a complex approach including chemical vapor deposition.[36] Hence, we have reported an effective method to use graphene oxide (GO) to achieve the direct stabilization of pristine CNTs in water via mild sonication.[37] The incorporated CNTs can greatly deter GO sheets from restacking while GO are able to simultaneously inhibit CNTs from aggregating.[38−40] Moreover, the resulting GO-CNT composites with excellent dispersibility in aqueous solution can be employed to fabricate self-standing

Received: September 27, 2015
Accepted: December 1, 2015
Published: December 1, 2015

DOI: 10.1021/acsami.5b09115
ACS Appl. Mater. Interfaces 2015, 7, 27823−27830

papers.[41−44] More importantly, the flexible graphene-CNT papers possess 3D nanoporous architectures, large specific surface area, and interconnected conductive networks, which are expected to be ideal frameworks for immobilization and confinement of electrochemically active materials.[45−47]

In this work, graphene-CNT composites are utilized as conductive matrixes for immobilization and confinement of ultrathin SnS_2 nanosheets (SnS_2 NSs). Flexible and binder-free graphene-CNT/SnS_2 (SGC) papers have been nicely fabricated by employing GO-CNT composites and SnS_2 NSs via a combination of vacuum filtration and thermal reduction. The SGC papers have porous architectures with ultrathin SnS_2 NSs homogeneously dispersed and confined within the interconnected graphene-CNT matrixes. As a result, the optimized SGC paper gives an enhanced specific capacity (1118.2 mA h g^{-1}) benefiting from cooperative interaction between SnS_2 and graphene-CNT matrixes: (1) unique structures with SnS_2 NSs confined inside the graphene-CNT composites can effectively prevent their aggregation and accommodate their volumetric expansion during the cycling process. (2) The graphene-CNT networks will improve the conductivity of papers by providing conductive networks to facilitate the transportation of charge and lithium ions. (3) The porous structures derived from CNTs and SnS_2 NSs incorporated between the graphene interlayers can enable fast diffusion of Li^+.

2. EXPERIMENTAL SECTION

2.1. Materials. Pristine CNTs were purchased from Chengdu Institute of Organic Chemistry. Natural graphite powder, and all other reagents were brought from Sinopharm Chemical Reagent Co. Ltd.

2.2. Preparation of SnS_2 Nanosheets. SnS_2 nanosheets (SnS_2 NSs) were prepared through a hydrothermal approach.[15] Typically, 2.5 mmol of tin(IV) chloride pentahydrate, 10 mmol of thioacetamide, and 40 mL of water were mixed and then put in a 50 mL Teflon autoclave for heating at 160 °C for 12 h. At last, yellow solid was cleaned with water and then dried.

2.3. Preparation of GO-CNT Dispersions. GO sheets was fabricated from graphite through modified Hummers method.[48] Stable dispersions of GO-CNT composites were synthesized according to our group's approach.[37] Briefly, pristine CNTs and dispersions of GO sheets are mixed and sonicated for 2 h. The proportion of GO by weight is two times that of CNTs. The unstabilized CNTs are got rid of by further centrifugation, and homogeneous dispersions of GO-CNT composites are fabricated.

2.4. Preparation of Graphene-CNT/SnS_2 Papers. From Figure 1, the flexible SGC papers were prepared via a facile vacuum filtration and calcination procedure. Typically, a certain amount of SnS_2 NS dispersions and GO-CNT dispersions were mixed by sonication for 2 h. Then, dispersions of GO-CNT composites and SnS_2 NSs were filtrated via a poly(vinylidene fluoride) film filter. In order to reduce GO to graphene, the as-prepared SnS_2/GO-CNT papers were calcined at 350 °C for 3 h under N_2 flow. The SGC papers with GO-CNT composites to SnS_2 mass ratio of 1/2, 2/1, and 1/1 are noted as SGC21, SGC12, and SGC11, respectively. Moreover, graphene-CNT (GC) papers and SnS_2/graphene (SG) papers were prepared by the aforementioned process without any SnS_2 or CNT. Correspondingly, the SG papers containing SnS_2 NSs and GO (1/1, w/w) were noted as SG11.

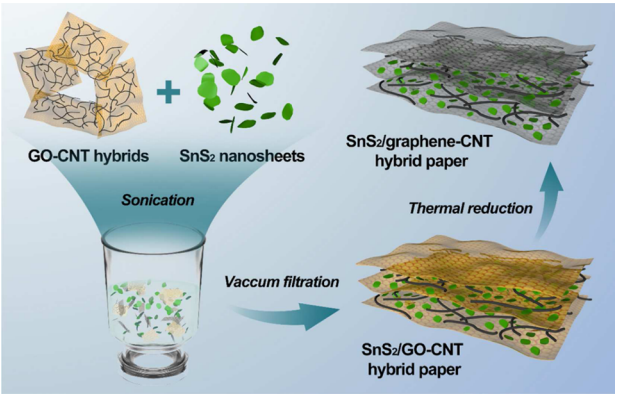

Figure 1. Schematic illustration of the preparation procedure of flexible self-standing graphene-CNT/SnS_2 hybrid paper.

2.5. Materials Characterization. Field emission scanning electron microscopy (FESEM) was conducted on FESEM, Ultra 55. Transmission electron microscopy (TEM) and high-resolution transmission electron microscopy (HRTEM) were conducted on a Tecnai G2 20 TWIN transmission electron microscope. X-ray diffraction (XRD) pattern was performed with an X'Pert Pro X-ray diffractometer with Cu Kα radiation (λ = 0.1542 nm) at a current of 40 mA and voltage of 40 kV. The Brunauer−Emmett−Teller (BET) analysis was performed via Belsorp-max surface area test instrument by N_2 physisorption at 77 K. X-ray photoelectron spectroscopy (XPS) measurements were investigated by a VG ESCALAB 220I-XL instrument.

2.6. Electrochemical Tests. Electrode materials were assembled into coin cells to study their electrochemical performance in an argon-filled glovebox. Celgard-2400 films were employed as separators, lithium foils as counter electrodes, and 1 M $LiPF_6$ in ethylene carbonate (EC)/dimethyl carbonate (DMC)/diethyl carbonate (DEC) (1:1:1, v/v/v) as the electrolytes. The working electrodes were binder-free SGC papers with no conductive additives and binders. In contrast, the SnS_2 NS anodes were fabricated through coating a slurry consisting of conductive carbon black, SnS_2 NSs, and poly(vinylidene fluoride) dispersed in *N*-methyl-2-pyrrolidinone (8:1:1, w/w/w) on copper foil. Cyclic voltammetry (CV) measurement and electrochemical impedance spectroscopy (EIS) were conducted via a CHI660D workstation (Chenhua Instruments Co. Ltd.). Galvanostatic discharge/charge tests and rate capacity at high current densities were investigated through a CT2013A device (LAND Electronic Co. Ltd.).

3. RESULTS AND DISCUSSION

3.1. Morphologies and Structures. SEM images in Figure 2a reveal that the lateral size of ultrathin SnS_2 NSs are uniformly from 10 to 30 nm. The corresponding TEM image in Figure 2b also verifies that the SnS_2 NSs are of nanosheet morphologies. More nanostructures of ultrathin SnS_2 NSs obtained from the HRTEM observation (Figure 2c) show a

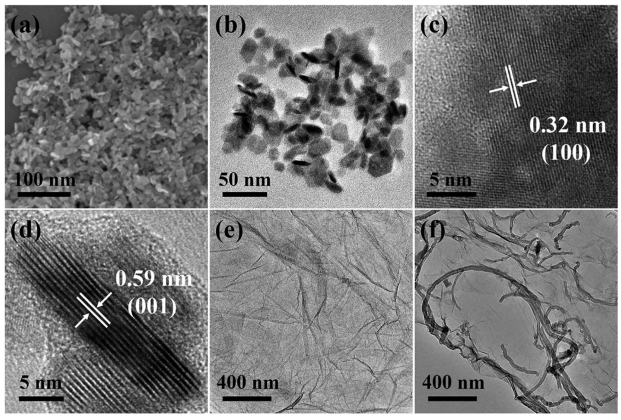

Figure 2. (a) FESEM and (b) TEM images of SnS_2 NSs. HRTEM images of (c) planar and (d) perpendicular SnS_2 NSs. TEM images of (e) GO sheets and (f) GO-CNT composites.

DOI: 10.1021/acsami.5b09115
ACS Appl. Mater. Interfaces 2015, 7, 27823−27830

planar nanosheet with the lattice interlayer of 0.32 nm, related to the (100) plane of SnS_2. From the HRTEM image of the perpendicular edges of SnS_2 NSs (Figure 2d), the SnS_2 NSs exhibit a typical lamellar structure with about 10 sandwiched S−Sn−S layers and interlayer lattice interlayer of 0.59 nm, which is indexed to the (001) plane of SnS_2. From Figure 2e, the sizes of GO sheets are usually a few micrometers. The AFM analysis of GO sheets (Supporting Information Figure S1) displays that GO sheets have a thickness of 1 nm. Due to the hydrophilic groups of the GO sheets (Figure 1), it readily forms stable dispersions of GO sheets through sonication, which can be employed to achieve direct stabilization of CNTs in water. There is a strong $\pi-\pi$ link between GO sheets and CNTs, where the oxygenated group are able to keep the outstanding dispersibility of GO-CNT composites.[37] As displayed in Figure 2f, hair-like original CNTs are tightly dispersed onto GO sheets. In the hybrids, GO sheets can greatly deter CNTs from aggregation while the CNTs can hinder GO sheets from restacking at the same time. Notably, both the ultrathin SnS_2 NSs and GO-CNT composites show excellent dispersibility in water (left and middle in Supporting Information Figure S2), and therefore the mixed dispersions of SnS_2 NSs and GO-CNT composites are very stable (right in Supporting Information Figure S2). Excellent dispersibility of SnS_2 NSs and GO-CNT composites in water is crucial for the fabrication of flexible self-standing SGC papers, which is favorable for the homogeneous dispersion of SnS_2 NSs within the graphene-CNT composites.

From Figure 1, flexible SGC papers are readily prepared via facile filtration of a mixed suspension of SnS_2 NSs and GO-CNT composites and subsequent thermal reduction of GO sheets. Panels a−d of Figure 3 display the cross-sectional

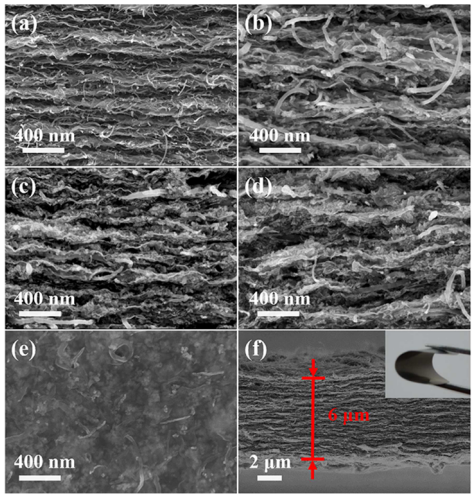

Figure 3. Cross-sectional FESEM images of (a) GC, (b) SGC12, (c) SGC11, and (d) SGC21 papers. (e) Top-view FESEM image of SGC11 paper. (f) Cross-sectional FESEM image of SGC11 paper at low magnification. The inset of panel f shows the digital photograph of flexible self-standing SGC11 paper.

FESEM images of GC, SGC12, SGC11, and SGC21 papers. It can be observed that all papers possess porous sandwiched structures while CNTs are incorporated within the graphene sheets. Moreover, the content of ultrathin SnS_2 NSs within SGC papers obviously decreases with increased weight ratios of graphene-CNT composites to SnS_2 NSs. As for SGC11 paper (Figure 3c), the SnS_2 NSs confined within the porous graphene-CNT composites can greatly prevent graphene sheets from restacking and deter their pulverization during the discharge−charge procedure. Simultaneously, the well-dispersed SnS_2 NSs are able to provide porous structures and enable swift diffusion of Li^+. However, an excessive amount of SnS_2 NSs in the SGC21 paper will result in severe agglomeration (Figure 3d). The top-view SEM image of SGC11 paper verifies the uniform dispersion of ultrathin SnS_2 NSs within the graphene-CNT matrixes (Figure 3e). Moreover, the EDS mapping analysis also confirms the uniform dispersion of tin, carbon, sulfur, and oxygen elements (Supporting Information Figure S3). The low amount of oxygen indicates successful reduction of graphene sheets after the calcination procedure.[49] As displayed in Figure 3f, the average thickness of SGC11 paper is about 6 μm, and it can be tunable by readily varying the amount of the mixed suspensions of SnS_2 NSs and GO-CNT composites for filtration. It is worthy to mention that no breakage is found after bending the flexible SGC11 paper back and forth (inset of Figure 3f). However, some fractures can be seen with further increased content of SnS_2 NSs in the papers. Thus, the porous structures and good mechanical flexibility of SGC papers are mainly resulted from the cooperative interactions of graphene-CNT composites and SnS_2 NSs.

From the TEM observation in Figure 4a,b, SnS_2 NSs and CNTs are uniformly confined within the high-surface-area

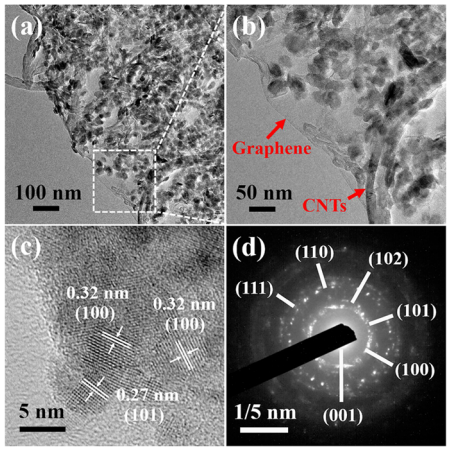

Figure 4. (a, b) TEM and (c) HRTEM images of SGC11 paper. (d) SAED pattern of SnS_2 NSs in the SGC11 paper.

graphene sheets. The confinement of SnS_2 NSs within GO-CNT hybrid frameworks can effectively prevent them from aggregation and inhibit their volumetric expansion during the cycling process. Supporting Information Figure S4 shows that the graphene sheets in SGC11 paper have one to two layers, which are attributed to the ultrathin layered SnS_2 NSs well-dispersed between the graphene layers. In the HRTEM image of SnS_2 NSs in SGC11 paper (Figure 4c), the lattice interlayers of 0.32 and 0.27 nm can be indexed to (100) and (101) planes of SnS_2, respectively. The SAED pattern (Figure 4d) reveals the polycrystalline structure of SnS_2 NSs, and the diffuse rings are attributed to (001), (100), (101), (102), (110), and (111) planes of SnS_2, respectively. These results unambiguously confirm the existence of SnS_2 NSs in the SGC papers.

The crystal structures of GO, CNTs, SnS_2 NSs, GO-CNT composites, GC, and SGC11 papers were studied using XRD as shown in Figure 5. GO exhibits a diffraction peak at $2\theta = 10.7°$ while CNTs show a diffraction peak at $2\theta = 26.2°$. Two peaks

DOI: 10.1021/acsami.5b09115
ACS Appl. Mater. Interfaces 2015, 7, 27823−27830

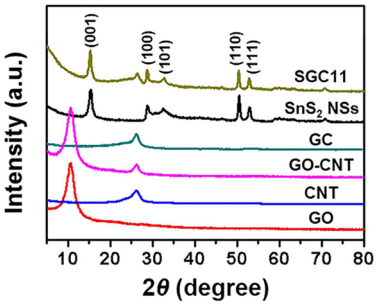

Figure 5. XRD patterns of GO, CNT, GO-CNT composites, SnS_2 NSs, GC, and SGC11 papers.

of GO-CNT composites located at 2θ = 10.7° and 26.2° indicate the integration of CNTs with GO sheets. Disappearance of the peak of GC paper located at 2θ = 10.7° confirms the highly reduced graphene sheets. Bare SnS_2 NSs show five diffraction peaks at 2θ = 15.3°, 28.8°, 32.5°, 50.4°, and 52.8°, corresponding to (001), (100), (101), (110), and (111) planes of SnS_2 (JCPDS No. 23-0667), respectively. The peaks of SGC11 paper suggests the coexistence of GC and SnS_2 NSs. Moreover, the XRD patterns of SGC21, SGC11, and SGC12 papers (Supporting Information Figure S5) all reveal the combination of GC and SnS_2 NSs. Additionally, the intensities of the peaks indexed to SnS_2 all decrease as the proportion of SnS_2 by weight within the SGC papers decreases.

The survey spectrum of SGC11 paper (Figure 6a) confirms the existence of C, Sn, O, and S elements within SGC11 paper. In the high-resolution Sn 3d spectrum, the peaks centered at 487.1 and 495.6 eV are related with Sn $3d_{5/2}$ and Sn $3d_{3/2}$ binding energies (Figure 6b). Notably, S $2p_{1/2}$ and S $2p_{3/2}$ orbitals of S^{2-} appear at 162.7 and 161.8 eV in the curves of Figure 6c, respectively. These outcomes are in good correspondence with previous literature about SnS_2.[50] High-resolution C 1s curves of GO-CNT composites and SGC11 paper are displayed in Figure 6d. From the C 1s spectra of GO-CNT composites, five peaks located at 284.5, 285.3, 286.8, 287.9, and 288.7 eV are indexed to sp^2 C, sp^3 C, -C−O, -C═O, and -COO groups, respectively. Contrarily, the intensities of oxygenated carbon peaks of SGC11 paper obviously decrease, indicating the removal of most oxygenated groups of GO sheets.

The BET analysis (Figure 7) indicates SnS_2 NSs as nonporous materials due to its repeatable type II isotherms.

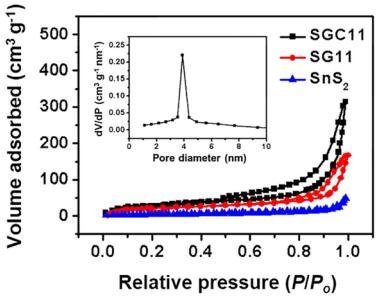

Figure 7. Nitrogen adsorption isotherms of SnS_2 NSs, SG11, and SGC11 papers. The inset shows the corresponding pore size distribution of the SGC11 paper.

The SGC11 and SG11 papers both exhibit IV isotherms, verifying the papers as mesoporous materials. The specific surface area of SnS_2 NSs and SGC11 and SG11 papers are summarized in Supporting Information Table S1. Notably, the specific surface areas of SGC11 and SG11 papers are 148.5 and 96.8 $m^2\ g^{-1}$, which reveals that the increased porosity and specific surface area owing to the incorporation of CNTs. The surface area of SGC11 paper is nearly 10 times higher than that (14.3 $m^2\ g^{-1}$) of bare SnS_2 NSs. This is mainly due to the porous architectures derived from graphene-CNT matrixes with open and continuous channels in the papers. Besides, the pore size distribution of SGC11 paper is centered at approximately 4 nm (inset of Figure 7), which is in the mesoporous range. The

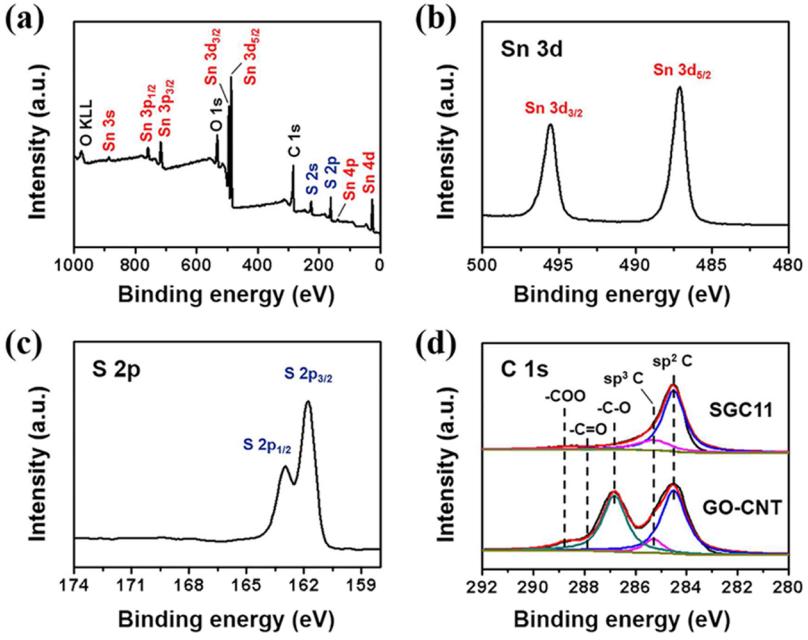

Figure 6. (a) XPS survey spectrum. High-resolution (b) Sn 3d spectrum and (c) S 2p spectrum of SGC11 paper. (d) C 1s spectra of SGC11 paper and GO-CNT composites.

DOI: 10.1021/acsami.5b09115
ACS Appl. Mater. Interfaces 2015, 7, 27823−27830

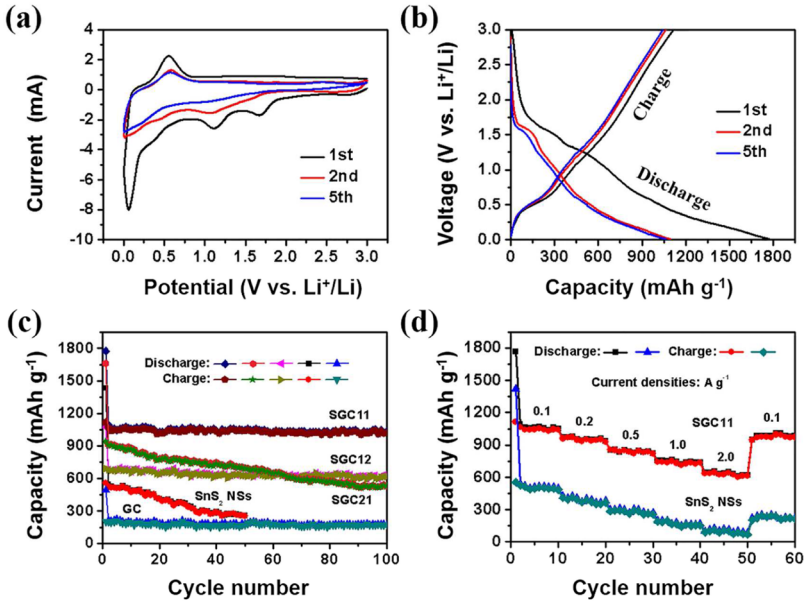

Figure 8. (a) CV curves (first, second, and fifth cycles) of SGC11 paper measured at a scan rate of 0.1 mV s^{-1}. (b) Discharge/charge curves of SGC11 paper in the first, second, and fifth cycles. (c) Cycling performance of SnS_2 NSs, GC, SGC21, SGC11, and SGC12 papers in the voltage range from 0.01 to 3.0 V at a current density of 0.1 A g^{-1}. (d) Rate performance of SnS_2 NSs and SGC11 paper at various current densities.

porous structures with higher specific surface area can enable fast diffusion of Li^+ and suppress the volume change of electroactive materials.

3.2. Electrochemical Performance. The electrochemistry of the discharge−charge process was investigated by conducting CV tests of SGC11 paper (Figure 8a). During the initial CV cycle, the peaks (1.12 and 1.68 V) are indexed to the transformation of SnS_2 to Sn and Li_2S according to eq 1.[51] And the reduction peak (0.30 V) is related with the generation of Li−Sn alloy via a conversion reaction based on eq 2. During the anodic process, one peak (0.56 V) is related with delithiation reaction of Li−Sn alloy (eq 2). In the following cycles, the insertion of Li^+ into Sn occurs at 0.9−1.1 V while the decomposition of Li−Sn alloy occurs at 0.4−0.7 V.

$$SnS_2 + 4Li^+ + 4e^- \rightarrow Sn + 2Li_2S \quad (1)$$

$$Sn + xLi^+ + xe^- \rightleftharpoons Li_xSn \qquad (0 \le x \le 4.4) \quad (2)$$

In the initial lithiation curve of SGC11 papers (Figure 8b), the potential plateaus (1.25 and 1.70 V) are attributed to lithiation of SnS_2 into Sn nanoparticles embedded in Li_2S matrix. During the charge process, the potential plateau (0.65 V) is indexed to the delithiation procedure of Li−Sn alloy (eq 2). As displayed in Figure 8b, the first discharge−charge specific capacities of SGC11 paper are 1774.3 and 1118.2 mA h g^{-1}, that is 37% for irreversible loss of the first cycle. Contrarily, initial charge−discharge capacities of bare SnS_2 NSs are 1434.5 and 556.3 mA h g^{-1}, that is, the first irreversible loss of 61%. These results reveal the graphene-CNT composites can greatly improve the reversible capacity and reduce the first irreversible loss of SGC paper, which resulted from the enhanced conductivity as well as less aggregation and pulverization of SnS_2 NSs in the long-term cycling procedure, therefore decreasing the first irreversible loss of SGC papers. Besides, the addition of binders for preparing SnS_2 electrode can also lead to a large first irreversible loss. By comparison, the binder-free SGC papers are able to fully utilize the active SnS_2 NSs and conductive graphene-CNT matrixes, thus leading to greatly enhanced specific capacity.

Figure 8c demonstrates the cyclic behaviors of SnS_2 NSs and GC and SGC papers. Neat GC paper manifests 190 mA h g^{-1} as well as outstanding cyclic behavior while the SnS_2 NS electrode exhibits continuous discharge capacity from 556.3 to 255.6 mA h g^{-1} at the 50th cycle. Fast decay of SnS_2 NSs mainly resulted from their bad conductivity, severe aggregation, and pulverization after a long cycling process.[52] In comparison, the SGC12, SGC11, and SGC21 papers deliver improved capacities of 611.3, 1017.5, and 552.4 mA h g^{-1} at the 100th cycle, respectively. Notably, SGC11 paper shows the highest specific capacity owing to the optimized amount of SnS_2 NSs incorporated within graphene-CNT matrixes. Even after the long-term cycling procedure, the SGC11 paper still maintains its original structure with almost unchanged thickness (Supporting Information Figure S6). These results verify that the graphene-CNT matrixes are able to effectively accommodate the large volumetric change of SnS_2 and maintain the structural stability. From Supporting Information Figure S7, the addition of CNTs can improve the conductivity and porosity for fast transportation of ions and lithium ions, thus achieving higher specific capacities of SGC11 papers than SG11 papers.

The rate capabilities of SnS_2 NSs and SGC11 paper (Figure 8d) tells that the SGC11 paper has an enhanced rate performance compared to that of bare SnS_2 NSs. Specifically, the reversible capacity of SnS_2 NSs exhibit about 80 mA h g^{-1} at 2 A g^{-1}, regaining 216 mA h g^{-1} as it reduces to 0.1 A g^{-1}, that is, 39% of the original capacity. In contrast, the SGC11 paper exhibits an improved capacity of 634.6 mA h g^{-1} at 2 A g^{-1}, restoring to 972 mAh g^{-1} as it goes back to 0.1 A g^{-1}, that is, 87% of the original capacity. From Supporting Information Figure S8, SGC11 paper delivers better rate behavior than SGC21 and SGC12 papers. Furthermore, the SGC11 paper exhibits good cyclic stability under high current densities (Figure 9) with its capacity retained at 798.5, 646.2, and 509.1 mA h g^{-1} at 0.5, 1, and 2 A g^{-1} at the 100th cycle.

DOI: 10.1021/acsami.5b09115
ACS Appl. Mater. Interfaces 2015, 7, 27823−27830

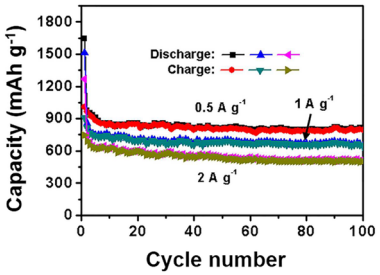

Figure 9. High-rate cycling performance of SGC11 paper in the voltage range from 0.01 to 3.0 V at current densities of 0.5, 1, and 2 A g^{-1}.

The excellent cycling behavior and rate performance of SGC11 paper is ascribed to the cooperative interactions between SnS_2 NSs and graphene-CNT composites. First, the ultrathin SnS_2 NSs are uniformly confined within graphene-CNT matrixes, which can stabilize the structures, deter SnS_2 NSs from aggregation, and suppress their volumetric change. Second, the graphene-CNT matrixes are able to enhance the conductivity and enable fast transportation of ions. Finally, the porous architectures derived from SnS_2 NSs well-dispersed within graphene-CNT matrixes are able to facilitate fast diffusion of Li^+.

To better understand the superior electrochemical performance of SGC papers, EIS tests of SnS_2 NSs and SGC11 and SG11 papers after 10 cycles are present in Figure 10. The

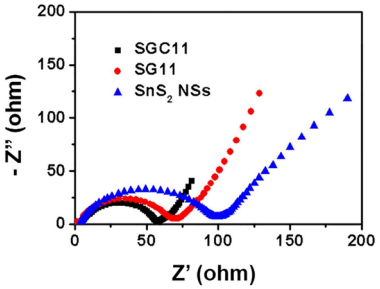

Figure 10. Nyquist plots of SnS_2 NSs, SG11, and SGC11 papers measured in the frequency range from 100 kHz to 0.01 Hz with an AC voltage amplitude of 5.0 mV.

Nyquist curves usually have one single semicircle at the high-frequency part as well as one straight line at the low-frequency part, indexed to the charge-transportation processes and the ion diffusion processes, respectively.[53] The radius of a semicircle of SGC11 paper at the high−medium frequency part is smaller than that of SnS_2 NSs, indicating its smaller contact and charge-transportation resistance, which directly confirm that the graphene-CNT matrixes can greatly provide fast transportation of Li^+. Owing to the addition of CNTs, the SGC11 electrode displays a smaller semicircle compared with that of SG11 electrode, which leads to its improved electrical conductivity and better lithium storage performance.

4. CONCLUSIONS

In summary, flexible self-standing graphene-CNT matrixes with porous structures and excellent electrical conductivity are utilized for immobilization and confinement of SnS_2 nanosheets. The resulting SGC papers with ultrathin SnS_2 NSs homogeneously dispersed and confined within interconnected graphene-CNT matrixes are able to effectively prevent their aggregation and pulverization. Additionally, the conductive graphene-CNT networks are able to greatly improve the conductivity of SGC papers. As a result, the optimized SGC paper exhibits improved performance (1118.2 mA h g^{-1}) as well as rate performance with 634.6 mA h g^{-1} at 2 A g^{-1}. The cooperative interactions between SnS_2 NSs and graphene-CNT matrixes contributes to the enhanced lithium storage performance of SGC papers. Thus, this report highlights the strategy to employ graphene-CNT composites for immobilization and confinement of various active materials to prepare flexible electrodes.

■ ASSOCIATED CONTENT

Supporting Information

The Supporting Information is available free of charge on the ACS Publications website at DOI: 10.1021/acsami.5b09115.

Specific surface areas of SnS_2 nanosheets and SGC11 and SG11 papers, AFM analysis of graphene oxide, digital images of suspensions of SnS_2 NSs, GO-CNT composites (2/1, w/w) and the mixed suspension of SnS_2 NSs and GO-CNT composites, top-view FESEM image, corresponding EDS spectrum, and EDS mapping images of SGC11 paper, XRD patterns of SGC21, SGC11, and SGC12 papers, cross-section FESEM image of SGC11 papers after the cycling test, cyclic performance of SGC11 and SG11 papers, and rate performance of SGC21, SGC11, and SGC12 papers at various current densities (PDF)

■ AUTHOR INFORMATION

Corresponding Authors

*(T.L.) E-mail: txliu@fudan.edu.cn. Tel.: +86-21-55664197. Fax: +86-21-65640293.

*(W.F.) E-mail: 12110440003@fudan.edu.cn.

Notes

The authors declare no competing financial interest.

■ ACKNOWLEDGMENTS

We are grateful for the financial support from the National Natural Science Foundation of China (Grants 51125011 and 51433001).

■ REFERENCES

(1) Arico, A. S.; Bruce, P.; Scrosati, B.; Tarascon, J. M.; Van Schalkwijk, W. Nanostructured Materials for Advanced Energy Conversion and Storage Devices. *Nat. Mater.* **2005**, *4*, 366−377.

(2) Cheng, F. Y.; Liang, J.; Tao, Z. L.; Chen, J. Functional Materials for Rechargeable Batteries. *Adv. Mater.* **2011**, *23*, 1695−1715.

(3) Sun, W. W.; Wang, Y. Graphene-Based Nanocomposite Anodes for Lithium-Ion Batteries. *Nanoscale* **2014**, *6*, 11528−11552.

(4) Liang, J.; Yu, X. Y.; Zhou, H.; Wu, H. B.; Ding, S. J.; Lou, X. W. Bowl-Like SnO_2@Carbon Hollow Particles as An Advanced Anode Material for Lithium-Ion Batteries. *Angew. Chem., Int. Ed.* **2014**, *53*, 12803−12807.

(5) Xu, X.; Fan, Z. Y.; Yu, X. Y.; Ding, S. J.; Yu, D. M.; Lou, X. W. A Nanosheets-on-Channel Architecture Constructed from MoS_2 and CMK-3 for High-Capacity and Long-Cycle-Life Lithium Storage. *Adv. Energy Mater.* **2014**, *4*, 1400902.

(6) Gao, G. X.; Lu, S. Y.; Dong, B. T.; Zhang, Z. C.; Zheng, Y. S.; Ding, S. J. One-Pot Synthesis of Carbon Coated Fe_3O_4 Nanosheets with Superior Lithium Storage Capability. *J. Mater. Chem. A* **2015**, *3*, 4716−4721.

(7) Zhu, C. B.; Mu, X. K.; van Aken, P. A.; Maier, J.; Yu, Y. Fast Li Storage in MoS_2-Graphene-Carbon Nanotube Nanocomposites:

DOI: 10.1021/acsami.5b09115
ACS Appl. Mater. Interfaces 2015, 7, 27823−27830

Advantageous Functional Integration of 0D, 1D, and 2D Nanostructures. *Adv. Energy Mater.* **2015**, *5*, 1401170.
(8) Zhou, X. S.; Yin, Y. X.; Cao, A. M.; Wan, L. J.; Guo, Y. G. Efficient 3D Conducting Networks Built by Graphene Sheets and Carbon Nanoparticles for High-Performance Silicon Anode. *ACS Appl. Mater. Interfaces* **2012**, *4*, 2824−2828.
(9) Huang, X.; Zeng, Z. Y.; Zhang, H. Metal Dichalcogenide Nanosheets: Preparation, Properties and Applications. *Chem. Soc. Rev.* **2013**, *42*, 1934−1946.
(10) Liu, S. Y.; Lu, X.; Xie, J.; Cao, G. S.; Zhu, T. J.; Zhao, X. B. Preferential c-Axis Orientation of Ultrathin SnS_2 Nanoplates on Graphene as High-Performance Anode for Li-Ion Batteries. *ACS Appl. Mater. Interfaces* **2013**, *5*, 1588−1595.
(11) Geng, H.; Kong, S. F.; Wang, Y. NiS Nanorod-Assembled Nanoflowers Grown on Graphene: Morphology Evolution and Li-Ion Storage Applications. *J. Mater. Chem. A* **2014**, *2*, 15152−15158.
(12) Zhang, L. S.; Fan, W.; Liu, T. X. A Flexible Free-Standing Defect-Rich MoS_2/Graphene/Carbon Nanotube Hybrid Paper as A Binder-Free Anode for High-Performance Lithium Ion Batteries. *RSC Adv.* **2015**, *5*, 43130−43140.
(13) Du, Y. C.; Zhu, X. S.; Zhou, X. S.; Hu, L. Y.; Dai, Z. H.; Bao, J. C. Co_3S_4 Porous Nanosheets Embedded in Graphene Sheets as High-Performance Anode Materials for Lithium and Sodium Storage. *J. Mater. Chem. A* **2015**, *3*, 6787−6791.
(14) Du, Y. C.; Zhu, X. S.; Si, L.; Li, Y. F.; Zhou, X. S.; Bao, J. C. Improving the Anode Performance of WS_2 through a Self-Assembled Double Carbon Coating. *J. Phys. Chem. C* **2015**, *119*, 15874−15881.
(15) Zhai, C. X.; Du, N.; Yang, H. Z. D. Large-Scale Synthesis of Ultrathin Hexagonal Tin Disulfide Nanosheets with Highly Reversible Lithium Storage. *Chem. Commun.* **2011**, *47*, 1270−1272.
(16) Zhai, C. X.; Du, N.; Zhang, H.; Yu, J. X.; Yang, D. R. Multiwalled Carbon Nanotubes Anchored with SnS_2 Nanosheets as High-Performance Anode Materials of Lithium-Ion Batteries. *ACS Appl. Mater. Interfaces* **2011**, *3*, 4067−4074.
(17) Zhuo, L. H.; Wu, Y. Q.; Wang, L. Y.; Yu, Y. C.; Zhang, X. B.; Zhao, F. Y. One-Step Hydrothermal Synthesis of SnS_2/Graphene Composites as Anode Material for Highly Efficient Rechargeable Lithium Ion Batteries. *RSC Adv.* **2012**, *2*, 5084−5087.
(18) Li, J. P.; Wu, P.; Lou, F. J.; Zhang, P.; Tang, Y. W.; Zhou, Y. M.; Lu, T. H. Mesoporous Carbon Anchored with SnS_2 Nanosheets as An Advanced Anode for Lithium-Ion Batteries. *Electrochim. Acta* **2013**, *111*, 862−868.
(19) Kim, T.-J.; Kim, C.; Son, D.; Choi, M.; Park, B. Novel SnS_2-Nanosheet Anodes for Lithium-Ion Batteries. *J. Power Sources* **2007**, *167*, 529−535.
(20) Ji, L.; Xin, H. L.; Kuykendall, T. R.; Wu, S.; Zheng, H. M.; Rao, M.; Cairns, E. J.; Battaglia, V.; Zhang, Y. G. SnS_2 Nanoparticle Loaded Graphene Nanocomposites for Superior Energy Storage. *Phys. Chem. Chem. Phys.* **2012**, *14*, 6981−6986.
(21) Yin, J. F.; Cao, H. Q.; Zhou, Z. F.; Zhang, J. X.; Qu, M. Z. SnS_2@reduced Graphene Oxide Nanocomposites as Anode Materials with High Capacity for Rechargeable Lithium Ion Batteries. *J. Mater. Chem.* **2012**, *22*, 23963−23970.
(22) Jiang, X.; Yang, X. L.; Zhu, Y.; Shen, J. H.; Fan, K. C.; Li, C. Z. In Situ Assembly of Graphene Sheets-Supported SnS_2 Nanoplates into 3D Macroporous Aerogels for High-Performance Lithium Ion Batteries. *J. Power Sources* **2013**, *237*, 178−186.
(23) Du, N.; Wu, X. L.; Zhai, C. X.; Zhang, H.; Yang, D. R. Large-Scale Synthesis and Application of SnS_2-Graphene Nanocomposites as Anode Materials for Lithium-Ion Batteries with Enhanced Cyclic Performance and Reversible Capacity. *J. Alloys Compd.* **2013**, *580*, 457−464.
(24) Zhang, Q. Q.; Li, R.; Zhang, M. M.; Zhang, B. L.; Gou, X. L. SnS_2/Reduced Graphene Oxide Nanocomposites with Superior Lithium Storage Performance. *Electrochim. Acta* **2014**, *115*, 425−433.
(25) Chen, P.; Su, Y.; Liu, H.; Wang, Y. Interconnected Tin Disulfide Nanosheets Grown on Graphene for Li Ion Storage and Photocatalytic Applications. *ACS Appl. Mater. Interfaces* **2013**, *5*, 12073−12082.
(26) Liu, Z. X.; Deng, H. Q.; Mukherjee, P. P. Evaluating Pristine and Modified SnS_2 as A Lithium-Ion Battery Anode: A First-Principles Study. *ACS Appl. Mater. Interfaces* **2015**, *7*, 4000−4009.
(27) Sun, Y. Q.; Wu, Q.; Shi, G. Q. Graphene Based New Energy Materials. *Energy Environ. Sci.* **2011**, *4*, 1113−1132.
(28) Tang, C.; Zhang, Q.; Zhao, M. Q.; Tian, G. L.; Wei, F. Resilient Aligned Carbon Nanotube/Graphene Sandwiches for Robust Mechanical Energy Storage. *Nano Energy* **2014**, *7*, 161−169.
(29) Fan, W.; Miao, Y. E.; Huang, Y. P.; Tjiu, W. W.; Liu, T. X. Flexible Free-Standing 3D Porous N-Doped Graphene-Carbon Nanotube Hybrid Paper for High-Performance Supercapacitors. *RSC Adv.* **2015**, *5*, 9228−9236.
(30) Byon, H. R.; Gallant, B. M.; Lee, S. W.; Shao-Horn, Y. Role of Oxygen Functional Groups in Carbon Nanotube/Graphene Free-standing Electrodes for High Performance Lithium Batteries. *Adv. Funct. Mater.* **2013**, *23*, 1037−1045.
(31) Tang, C.; Zhang, Q.; Zhao, M. Q.; Huang, J. Q.; Cheng, X. B.; Tian, G. L.; Peng, H. J.; Wei, F. Nitrogen-Doped Aligned Carbon Nanotube/Graphene Sandwiches: Facile Catalytic Growth on Bifunctional Natural Catalysts and Their Applications as Scaffolds for High-Rate Lithium-Sulfur Batteries. *Adv. Mater.* **2014**, *26*, 6100.
(32) Shen, L. F.; Zhang, X. G.; Li, H. S.; Yuan, C. Z.; Cao, G. Z. Design and Tailoring of A Three-Dimensional TiO_2-Graphene-Carbon Nanotube Nanocomposite for Fast Lithium Storage. *J. Phys. Chem. Lett.* **2011**, *2*, 3096−3101.
(33) Cheng, Q.; Tang, J.; Ma, J.; Zhang, H.; Shinya, N.; Qin, L. C. Graphene and Carbon Nanotube Composite Electrodes for Supercapacitors with Ultra-High Energy Density. *Phys. Chem. Chem. Phys.* **2011**, *13*, 17615−17624.
(34) Peng, H. J.; Huang, J. Q.; Zhao, M. Q.; Zhang, Q.; Cheng, X. B.; Liu, X. Y.; Qian, W. Z.; Wei, F. Nanoarchitectured Graphene/CNT@Porous Carbon with Extraordinary Electrical Conductivity and Interconnected Micro/Mesopores for Lithium-Sulfur Batteries. *Adv. Funct. Mater.* **2014**, *24*, 2772−2781.
(35) Hu, Y. H.; Li, X. F.; Wang, J. J.; Li, R. Y.; Sun, X. L. Free-Standing Graphene-Carbon Nanotube Hybrid Papers Used as Current Collector and Binder Free Anodes for Lithium Ion Batteries. *J. Power Sources* **2013**, *237*, 41−46.
(36) Park, H. W.; Lee, D. U.; Liu, Y. L.; Wu, J. S.; Nazar, L. F.; Chen, Z. W. Bi-Functional N-Doped CNT/Graphene Composite as Highly Active and Durable Electrocatalyst for Metal Air Battery Applications. *J. Electrochem. Soc.* **2013**, *160*, A2244−A2250.
(37) Zhang, C.; Ren, L. L.; Wang, X. Y.; Liu, T. X. Graphene Oxide-Assisted Dispersion of Pristine Multiwalled Carbon Nanotubes in Aqueous Media. *J. Phys. Chem. C* **2010**, *114*, 11435−11440.
(38) Zhang, C.; Tjiu, W. W.; Liu, T. X. All-Carbon Composite Paper as A Flexible Conducting Substrate for the Direct Growth of Polyaniline Particles and Its Applications in Supercapacitors. *Polym. Chem.* **2013**, *4*, 5785−5792.
(39) Yang, S. Y.; Chang, K. H.; Tien, H. W.; Lee, Y. F.; Li, S. M.; Wang, Y. S.; Wang, J. Y.; Ma, C.; Hu, C. C. Design and Tailoring of A Hierarchical Graphene-Carbon Nanotube Architecture for Supercapacitors. *J. Mater. Chem.* **2011**, *21*, 2374−2380.
(40) Peng, L. W.; Feng, Y. Y.; Lv, P.; Lei, D.; Shen, Y. T.; Li, Y.; Feng, W. Transparent, Conductive, and Flexible Multiwalled Carbon Nanotube/Graphene Hybrid Electrodes with Two Three-Dimensional Microstructures. *J. Phys. Chem. C* **2012**, *116*, 4970−4978.
(41) Lu, X. J.; Dou, H.; Gao, B.; Yuan, C. Z.; Yang, S. D.; Hao, L.; Shen, L. F.; Zhang, X. G. A Flexible Graphene/Multiwalled Carbon Nanotube Film as A High Performance Electrode Material for Supercapacitors. *Electrochim. Acta* **2011**, *56*, 5115−5121.
(42) Cheng, Y. W.; Lu, S. T.; Zhang, H. B.; Varanasi, C. V.; Liu, J. Synergistic Effects from Graphene and Carbon Nanotubes Enable Flexible and Robust Electrodes for High-Performance Supercapacitors. *Nano Lett.* **2012**, *12*, 4206−4211.
(43) Huang, Z. D.; Zhang, B. A.; Oh, S. W.; Zheng, Q. B.; Lin, X. Y.; Yousefi, N.; Kim, J. K. Self-Assembled Reduced Graphene Oxide/Carbon Nanotube Thin Films as Electrodes for Supercapacitors. *J. Mater. Chem.* **2012**, *22*, 3591−3599.

DOI: 10.1021/acsami.5b09115
ACS Appl. Mater. Interfaces 2015, 7, 27823−27830

(44) Tan, Y. Q.; Song, Y. H.; Zheng, Q. Facile Regulation of Glutaraldehyde-Modified Graphene Oxide for Preparing Free-Standing Papers and Nanocomposite Films. *Chin. J. Polym. Sci.* **2013**, *31*, 399−406.
(45) Yuan, C. Z.; Yang, L.; Hou, L. R.; Li, J. Y.; Sun, Y. X.; Zhang, X. G.; Shen, L. F.; Lu, X. J.; Xiong, S. L.; Lou, X. W. Flexible Hybrid Paper Made of Monolayer Co_3O_4 Microsphere Arrays on rGO/CNTs and Their Application in Electrochemical Capacitors. *Adv. Funct. Mater.* **2012**, *22*, 2560−2566.
(46) Han, K.; Liu, Z.; Ye, H. Q.; Dai, F. Flexible Self-Standing Graphene-Se@CNT Composite Film as A Binder-Free Cathode for Rechargeable Li-Se Batteries. *J. Power Sources* **2014**, *263*, 85−89.
(47) Huang, J. Q.; Peng, H. J.; Liu, X. Y.; Nie, J. Q.; Cheng, X. B.; Zhang, Q.; Wei, F. Flexible All-Carbon Interlinked Nanoarchitectures as Cathode Scaffolds for High-Rate Lithium-Sulfur Batteries. *J. Mater. Chem. A* **2014**, *2*, 10869−10875.
(48) Hummers, W. S.; Offeman, R. E. Preparation of Graphitic Oxide. *J. Am. Chem. Soc.* **1958**, *80*, 1339.
(49) Lu, J. L.; Liu, W. S.; Ling, H.; Kong, J. H.; Ding, G. Q.; Zhou, D.; Lu, X. H. Layer-by-Layer Assembled Sulfonated-Graphene/Polyaniline Nanocomposite Films: Enhanced Electrical and Ionic Conductivities, and Electrochromic Properties. *RSC Adv.* **2012**, *2*, 10537−10543.
(50) Jiang, Z. F.; Wang, C.; Du, G. H.; Zhong, Y. J.; Jiang, J. Z. In Situ Synthesis of SnS_2@Graphene Nanocomposites for Rechargeable Lithium Batteries. *J. Mater. Chem.* **2012**, *22*, 9494−9496.
(51) Luo, B.; Fang, Y.; Wang, B.; Zhou, J. S.; Song, H. H.; Zhi, L. J. Two Dimensional Graphene-SnS_2 Hybrids with Superior Rate Capability for Lithium Ion Storage. *Energy Environ. Sci.* **2012**, *5*, 5226−5230.
(52) Chang, K.; Wang, Z.; Huang, G. C.; Li, H.; Chen, W. X.; Lee, J. Y. Few-Layer SnS_2/Graphene Hybrid with Exceptional Electrochemical Performance as Lithium-Ion Battery Anode. *J. Power Sources* **2012**, *201*, 259−266.
(53) Kong, J. H.; Yee, W. A.; Yang, L. P.; Wei, Y. F.; Phua, S. L.; Ong, H. G.; Ang, J. M.; Li, X.; Lu, X. H. Highly Electrically Conductive Layered Carbon Derived from Polydopamine and Its Functions in SnO_2-Based Lithium Ion Battery Anodes. *Chem. Commun.* **2012**, *48*, 10316−10318.

DOI: 10.1021/acsami.5b09115
ACS Appl. Mater. Interfaces 2015, 7, 27823−27830